Denia Guzmán, FD.; Sánchez Orgaz, EM.; Martínez Casas, J. (2015). Finite element based acoustic analysis of dissipative silencers with high temperature and thermal-induced heterogeneity. Finite Elements in Analysis and Design. 101(1):46-57. doi:10.1016/j.finel.2015.04.004.

Finite element based acoustic analysis of dissipative silencers with high temperature and thermal-induced heterogeneity

F. D. Denia[a,], E. M. Sánchez-Orgaz[a], J. Martínez-Casas[a]*

[a]Centro de Investigación de Tecnología de Vehículos, Universitat Politècnica de València, Camino de Vera s/n, 46022 Valencia, Spain

R. Kirby[b]

[b]School of Engineering and Design, Mechanical Engineering, Brunel University, Uxbridge, Middlesex UB8 3PH, UK

***Corresponding author:**

Dr. F. D. Denia
Centro de Investigación de Tecnología de Vehículos
Universitat Politècnica de València
Camino de Vera s/n
46022 Valencia
Spain
Tel: + 34 96 387 70 07 Ext: 76225
Fax: + 34 96 387 76 29
e-mail: fdenia@mcm.upv.es

ABSTRACT

A mixed finite element model has been derived for the acoustic analysis of perforated dissipative silencers including several effects simultaneously: (1) High temperature and thermal gradients in the central duct and the outer absorbent material; (2) A perforated passage carrying non-uniform axial mean flow. For such a combination, the properties of sound propagation media and flow are inhomogeneous and vary with position. The material of the outer chamber can be modelled by its complex equivalent acoustic properties, which completely determine the propagation of sound waves in the air contained in the absorbent medium. Temperature gradients introduce variations in these properties that can be evaluated through a heterogeneous temperature-dependent resistivity in combination with material models obtained at room temperature. A pressure-based wave equation for stationary medium is then used with the equivalent density and speed of sound of the absorbent material varying as functions of the spatial coordinates. Regarding the central air passage, a wave equation in terms of acoustic velocity potential can be used to model the non-uniform moving medium since the presence of temperature variations introduce not only heterogeneous acoustic properties of the air but also a gradient in the mean flow velocity. The acoustic connection between the central passage and the outer chamber is given by the acoustic impedance of the perforated duct. This impedance depends on the heterogeneous properties of the absorbent material and the non-uniform mean flow, leading to a spatial variation of the acoustic coupling and also to additional convective terms in the governing equations. The results presented show the influence of temperature, thermal gradients and mean flow on the transmission loss of automotive silencers. It has been found that high temperature and thermal-induced heterogeneity can have a significant influence on the acoustic attenuation of an automotive silencer and so should be included in theoretical models. In some particular configurations it may be relatively accurate to approximate the temperature field by using a uniform profile with an average value, specially for low resistivity materials. It has been shown, however, that this is not always possible and attenuation overestimation is likely to be predicted, mainly for high radial thermal gradients and high material flow resistivities, if the temperature distribution is not taken into account.

Keywords: FEM; silencer; acoustics; high temperature; gradient; absorbent material; heterogeneity; flow

1. INTRODUCTION

The presence of high temperature and heterogeneous properties in dissipative silencers modifies their acoustic attenuation performance. These spatial variations can arise, for example, from uneven filling processes [1-4], non-uniform mean flow fields [5] and thermal gradients [6,7]. In the latter case, the difficulties associated with experimental measurements at high temperatures make it necessary to find computational approaches useful to evaluate the acoustic behaviour of the silencer.

Several theoretical models were developed to incorporate the influence of high temperature and thermal variations in ducts. Dong and Liu [8] presented a finite element approach for rectangular ducts including flow and temperature gradient. Prasad and Crocker [9] considered a wave equation with uniform mean flow in terms of velocity potential and obtained analytically the four-pole parameters for a straight pipe in the presence of a linear temperature gradient. Munjal and Prasad [10] noted that a temperature gradient would introduce a corresponding variation in the mean density and a gradient in the mean flow velocity and Mach number, and incorporated this influence in a plane wave propagation model for a uniform pipe. Sujith [11] presented a formulation for uniform ducts with arbitrarily large temperature gradients in the absence of flow, while Dokumaci [12] and Karthik *et al.* [13] extended the one-dimensional approach to include the presence of mean flow.

Significant temperature variations can be found along the exhaust system of internal combustion engines [14-18]. Concerning the acoustic performance of silencers, it is straightforward to account for the effects of uniform high temperature fields if only reactive elements are present [19], since attenuation curves at different temperatures overlap when a normalized frequency f/c is considered, c being the speed of sound at working temperature T [20]. Therefore, a single computation at a known temperature allows the calculation of the acoustic attenuation performance for a wide temperature range. The previous comments cannot be applied, in general, to dissipative silencers, since the acoustic properties of the absorbent material cannot be scaled in the same way [6,7]. This indicates that the approach considered for reactive configurations cannot be used to

describe sound propagation in the presence of a dissipative medium. In this case, a specific calculation is required for each temperature.

For reactive configurations, a number of works can be found where the influence of temperature and the associated gradients has been modelled and analysed. Kim *et al.* [21] presented a multidimensional analytical approach for the acoustic modelling of expansion chambers with mean flow and a temperature gradient. A segmentation technique was applied dividing the silencer into segments with constant temperature and mean flow, and matching the acoustic fields through the corresponding continuity conditions. The approach was extended by Kim and Choi [22] to circular reversing chambers with temperature variations and a stationary medium. Wang *et al.* [23] combined the segmentation procedure and the boundary element method (BEM) to compute the transmission loss of expansion chambers with uniform mean flow and a linear temperature gradient. Siano [24] presented some three-dimensional BEM results for perforated silencers with different uniform temperatures. It is worth noting that, for a continuously varying temperature field, a suitable version of the wave equation is required to account for the heterogeneous properties of the propagation medium [25,26]. For reactive configurations, this wave equation provides a model for computing the sound attenuation, once the coordinate-dependent density and speed of sound have been evaluated from the ideal gas law [7,27].

Few articles in the literature consider the effect of temperature on the performance of dissipative silencers. In principle, the equivalent bulk acoustic properties of fibres can be estimated by including the effect of temperature on the material resistivity [20]. This approach was experimentally validated by Christie [28], who predicted with reasonable agreement the characteristic impedance and propagation constant of mineral wool fibrous material at different temperatures from the combination of the flow resistivity measurements at those temperatures and a modified version of Delany and Bazley's formulae [29,30]. Williams et al. [31] have recently provided further experimental validation at high temperatures for additional fibrous materials such as basalt wool and E glass. From an acoustical point of view, a suitable material model can be obtained by using the results obtained at room conditions while updating the material resistivity to the actual working temperature. Concerning dissipative silencers, Ref. [6] presented a mode matching–based multidimensional analytical approach to assess thermal effects on the

acoustic performance of circular dissipative reversing chamber silencers. A significant temperature influence was found on the sound attenuation characteristics. To account for the temperature-induced heterogeneity within the absorbent material, a segmentation procedure was considered with a number of dissipative regions with different but axially uniform temperature. The regression formulas (similar to Delany and Bazley expressions) for texturized fibre glass at room conditions [32] were extended to high temperature applications by including the thermal influence on the material resistivity while keeping the rest of coefficients and exponents constant. The same procedure was applied in Ref. [7], where a numerical approach based on the finite element method (FEM) was presented to analyze the effect of a continuously varying temperature field on the transmission loss of perforated dissipative silencers. A suitable version of the wave equation was required to account for heterogeneous density and speed of sound [3,4,25,26]. In the previous approaches [6,7,31], the effect of the temperature on the acoustic properties of the absorbent material were accounted for by modifying the steady air-flow resistivity in the initial model of the material obtained at room temperature.

More general problems involving the simultaneous consideration of variable temperature and mean flow effects for perforated dissipative silencers containing an absorbent material require further research. The objective of the present work is to model and analyse the sound propagation in dissipative configurations including: (1) a central perforated passage carrying a non-uniform mean flow, and (2) high temperature and thermal variations in the central duct and the outer chamber. A mixed finite element approach is developed in the current investigation that couples a convective wave equation for inhomogeneous moving medium (in terms of an acoustic velocity potential) associated with the central duct and a pressure-based wave equation for heterogeneous stationary medium corresponding to the dissipative region. The influence of a number of parameters on the acoustic attenuation performance is investigated, including the effect of temperature, axial and radial thermal gradients and mean flow Mach number.

2. MATHEMATICAL APPROACH

Fig. 1 shows the sketch of a dissipative silencer, which consists of a perforated central duct (subdomain Ω_a) carrying a mean flow and an outer chamber (subdomain Ω_m) with absorbent material. The corresponding boundary surfaces are denoted by Γ_a and Γ_m, respectively, the inlet and outlet sections are represented by Γ_i and Γ_o, and the perforated

surface is Γ_p. The temperature field is assumed one-dimensional in the central passage, reaching its maximum value at the inlet while decreasing gradually along the flow path [14,16,17,18,21,23]. A more general multidimensional function $T(x,y,z) = T(\mathbf{x})$ is considered in the chamber [17]. Temperature variations in the silencer lead to heterogeneous properties in the propagation media as well as spatial dependence of the acoustic impedance $\tilde{Z}_p$ corresponding to the perforated duct. Sound propagation in Ω_a (air) is characterized by the axially-varying acoustic properties $\rho_a(x)$ and $c_a(x)$ (density and speed of sound, respectively). The corresponding multidimensional equivalent acoustic values $\rho_m(\mathbf{x})$ and $c_m(\mathbf{x})$ are used in the dissipative region Ω_m. Further details on these temperature-induced heterogeneities will be provided in sections 3.1 and 3.2.

It is worth noting that the variation of the mean density in the central duct due to the temperature gradient introduces a corresponding variation in the mean flow velocity and Mach number [10]. As can be seen in the figure, these axial variations of the mean flow velocity U_{mf} induced by the thermal gradient are also considered.

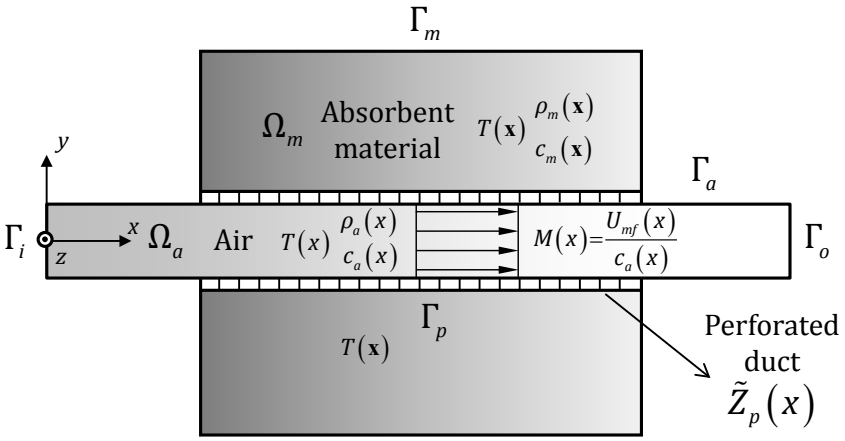

Figure 1 – Dissipative silencer with temperature variations and non-uniform mean flow.

2.1. Wave propagation in the central passage

In a continuously varying temperature field, a suitable version of the wave equation is required to account for the heterogeneous properties of the air. For uniform mean flow and a constant density ρ_a and speed of sound c_a, a simple and concise convective wave equation can be used in terms of the acoustic perturbation to the pressure field [33]. An equation of comparable simplicity cannot be used, however, when the medium is moving and the corresponding velocity field varies with position [25]. In this latter case, a

pressure-based wave equation includes spatial derivatives of the acoustic velocity, and therefore several dependent variables are involved. The problem can be overcome if an acoustic velocity potential-based wave equation is considered, as shown in the work of Pierce [25], where a generalization of the fundamental acoustic wave equation is derived. For the central passage depicted in Fig. 1, sound propagation is then governed by

$$\nabla\left(\rho_a \nabla\Phi_a\right)-\rho_a \mathrm{D}_t\left(\frac{1}{c_a^2}\mathrm{D}_t\Phi_a\right)=0 \tag{1}$$

where an inhomogeneous fluid (air) with ambient properties and flow that vary with position are considered. In Eq. (1), Φ_a is the acoustic velocity potential so that

$$\mathbf{U}_a=\left\{U_a \quad V_a \quad W_a\right\}^T=\nabla\Phi_a \tag{2}$$

and D_t is the total time derivative given by [25,33]

$$\mathrm{D}_t=\frac{\partial}{\partial t}+\mathbf{U}_{mf}^T\ \nabla \tag{3}$$

with $\mathbf{U}_{mf}=\left\{U_{mf} \quad V_{mf} \quad W_{mf}\right\}^T$. The relation between the acoustic pressure and the potential is given by [25]

$$P_a=-\rho_a \mathrm{D}_t\Phi_a \tag{4}$$

Similarly to earlier studies [33-35], the mean flow is assumed unidirectional, with $U_{mf} \neq 0$, $V_{mf} = W_{mf} = 0$, and transversely uniform over the duct cross-section. Therefore, no dependence exists on the (y, z) coordinates. As indicated previously, mean flow inhomogeneity is considered, however, along the axial direction, due to the presence of a temperature gradient in the perforated central passage, thus leading to $U_{mf} = U_{mf}$ (x). Therefore, the total time derivative can be written as

$$\mathrm{D}_t=\frac{\partial}{\partial t}+U_{mf}\frac{\partial}{\partial x}=\mathrm{j}\omega+U_{mf}\frac{\partial}{\partial x} \tag{5}$$

where a harmonic time dependence of the acoustic velocity potential is assumed, ω being the angular frequency and j the imaginary unit.

After applying the previous definition, Eq. (1) yields

$$\nabla\left(\rho_a \nabla\Phi_a\right)-\frac{\rho_a U_{mf}^2}{c_a^2}\frac{\partial^2\Phi_a}{\partial x^2}-\frac{2\rho_a \mathrm{j}\omega U_{mf}}{c_a^2}\frac{\partial\Phi_a}{\partial x}-\rho_a U_{mf}^2\frac{\partial\left(1/c_a^2\right)}{\partial x}\frac{\partial\Phi_a}{\partial x} \\ -\frac{\rho_a U_{mf}}{c_a^2}\frac{\partial U_{mf}}{\partial x}\frac{\partial\Phi_a}{\partial x}-\rho_a \mathrm{j}\omega U_{mf}\frac{\partial\left(1/c_a^2\right)}{\partial x}\Phi_a+\frac{\rho_a\omega^2}{c_a^2}\Phi_a=0 \tag{6}$$

The weighted residual statement (with weighting function Ψ) and the divergence theorem [36] are applied to Eq. (6). Further manipulation yields

$$-\int_{\Omega_a}\rho_a \nabla^T\Psi\mathbf{M}\nabla\Phi_a\,\mathrm{d}\Omega+\int_{\Omega_a}\Psi\left(\frac{U_{mf}^2}{c_a^2}\frac{\partial\rho_a}{\partial x}+\frac{\rho_a U_{mf}}{c_a^2}\frac{\partial U_{mf}}{\partial x}-\frac{2\rho_a \mathrm{j}\omega U_{mf}}{c_a^2}\right)\frac{\partial\Phi_a}{\partial x}\mathrm{d}\Omega \\ +\int_{\Omega_a}\Psi\left(-\rho_a \mathrm{j}\omega U_{mf}\frac{\partial\left(1/c_a^2\right)}{\partial x}+\frac{\rho_a\omega^2}{c_a^2}\right)\Phi_a\,\mathrm{d}\Omega+\int_{\Gamma_a}\rho_a\Psi\mathbf{n}^T\mathbf{M}\nabla\Phi_a\,\mathrm{d}\Gamma=0 \tag{7}$$

where it is worth noting that ρ_a, c_a and U_{mf} are variable functions. In Eq. (7), **n** is the outward unit normal vector to the boundary Γ and **M** is given by

$$\mathbf{M}=\begin{bmatrix}1-\dfrac{U_{mf}^2}{c_a^2} & 0 & 0\\ 0 & 1 & 0\\ 0 & 0 & 1\end{bmatrix} \tag{8}$$

After comparison of Eqs. (6) and (7), it is found that the product of the spatial derivatives of both the speed of sound and the acoustic velocity potential cancels during the mathematical procedure. In addition, since the ambient values satisfy the relation ρ_a U_{mf} S = *constant* [10] and the cross-section S of the central passage is uniform, the following expression can be obtained

$$U_{mf}\frac{\partial\rho_a}{\partial x}+\rho_a\frac{\partial U_{mf}}{\partial x}=0 \tag{9}$$

Therefore, the first two terms of the second integral in Eq. (7) also vanish and therefore the equation can be written as

$$-\int_{\Omega_a}\rho_a\nabla^T\Psi\mathbf{M}\nabla\Phi_a\,\mathrm{d}\Omega+\int_{\Omega_a}\Psi\left(-\frac{2\rho_a\,\mathrm{j}\omega U_{mf}}{c_a^2}\right)\frac{\partial\Phi_a}{\partial x}\mathrm{d}\Omega$$
$$+\int_{\Omega_a}\Psi\left(-\rho_a\,\mathrm{j}\omega U_{mf}\frac{\partial\left(1/c_a^2\right)}{\partial x}+\frac{\rho_a\omega^2}{c_a^2}\right)\Phi_a\,\mathrm{d}\Omega+\int_{\Gamma_a}\rho_a\,\Psi\mathbf{n}^T\mathbf{M}\nabla\Phi_a\,\mathrm{d}\Gamma=0 \tag{10}$$

The finite element discretization and interpolation (with shape functions **N**) are used in combination with the Galerkin approach [36], leading to

$$\sum_{e=1}^{N_a^e}\left(\int_{\Omega_a^e}\rho_a\left(\nabla\mathbf{N}\right)^T\mathbf{M}\nabla\mathbf{N}\,\mathrm{d}\Omega+\mathrm{j}\omega\int_{\Omega_a^e}\frac{2\rho_a U_{mf}}{c_a^2}\mathbf{N}^T\frac{\partial\mathbf{N}}{\partial x}\mathrm{d}\Omega+\mathrm{j}\omega\int_{\Omega_a^e}\rho_a U_{mf}\frac{\partial\left(1/c_a^2\right)}{\partial x}\mathbf{N}^T\mathbf{N}\,\mathrm{d}\Omega\right.$$
$$\left.-\omega^2\int_{\Omega_a^e}\frac{\rho_a}{c_a^2}\mathbf{N}^T\mathbf{N}\,\mathrm{d}\Omega\right)\tilde{\mathbf{\Phi}}_a^e=\sum_{e=1}^{N_a^e}\int_{\Gamma_a^e}\rho_a\mathbf{N}^T\mathbf{n}^T\mathbf{M}\nabla\Phi_a\,\mathrm{d}\Gamma \tag{11}$$

where signs have been change for convenience. $\tilde{\mathbf{\Phi}}_a^e$ contains the unknown nodal potentials and N_a^e represents the number of elements of subdomain Ω_a (air). Eq. (11) can be written in compact form as

$$\left(\mathbf{K}_a+\mathrm{j}\omega\left(\mathbf{C}_{a1}+\mathbf{C}_{a2}\right)-\omega^2\mathbf{M}_a\right)\tilde{\mathbf{\Phi}}_a=\mathbf{F}_a \tag{12}$$

where the following nomenclature has been introduced

$$\mathbf{K}_a=\sum_{e=1}^{N_a^e}\int_{\Omega_a^e}\rho_a\left(\nabla\mathbf{N}\right)^T\mathbf{M}\nabla\mathbf{N}\,\mathrm{d}\Omega,\qquad\mathbf{M}_a=\sum_{e=1}^{N_a^e}\int_{\Omega_a^e}\frac{\rho_a}{c_a^2}\mathbf{N}^T\mathbf{N}\,\mathrm{d}\Omega \tag{13,14}$$

$$\mathbf{C}_{a1}=\sum_{e=1}^{N_a^e}\int_{\Omega_a^e}\frac{2\rho_a U_{mf}}{c_a^2}\mathbf{N}^T\frac{\partial\mathbf{N}}{\partial x}\mathrm{d}\Omega,\qquad\mathbf{C}_{a2}=\sum_{e=1}^{N_a^e}\int_{\Omega_a^e}\rho_a U_{mf}\frac{\partial\left(1/c_a^2\right)}{\partial x}\mathbf{N}^T\mathbf{N}\,\mathrm{d}\Omega \tag{15,16}$$

$$\mathbf{F}_a=\sum_{e=1}^{N_a^e}\int_{\Gamma_a^e}\rho_a\mathbf{N}^T\mathbf{n}^T\mathbf{M}\nabla\Phi_a\,\mathrm{d}\Gamma=\sum_{e=1}^{N_a^e}\left(\int_{\Gamma_a^e\cap\Gamma_{bc}}\rho_a\mathbf{N}^T\left(1-\frac{U_{mf}^2}{c_a^2}\right)\frac{\partial\Phi_a}{\partial n}\mathrm{d}\Gamma+\int_{\Gamma_a^e\cap\Gamma_p}\rho_a\mathbf{N}^T\frac{\partial\Phi_a}{\partial n}\mathrm{d}\Gamma\right) \tag{17}$$

$\Gamma_{bc}=\Gamma_i\cup\Gamma_o$ being the surface where inlet/outlet boundary conditions are applied (see Fig. 1 for details).

It is worth noting that some differences arise in the formulation compared to Ref. [4] due to the spatial variation of the air properties. For a given temperature distribution, mass conservation is considered to compute the axial variation of U_{mf} [10,12] for a prescribed inlet mean flow Mach number M_i. The density and speed of sound ρ_a and c_a can be easily evaluated at each integration point assuming the ideal gas law, as shown in the

work of Dokumaci [12], where the local dependence of c_a and ρ_a on the mean flow velocity is not taken into account since the flow velocities under consideration are relatively low. The spatial derivative of c_a in Eq. (16) can be also calculated analytically and/or numerically, depending on the complexity of the temperature field. As can be inferred from the definition of $\mathbf{C}_{a2}$, the influence of this latter matrix on the silencer transmission loss is small when compared to the contributions from the rest of finite element matrices (this is also supported by additional calculations carried out by the authors with a number of parameters and temperature gradients).

2.2. Wave propagation in the outer chamber

In the absence of mean flow, the wave propagation in the heterogeneous absorbent material is governed by [3,4,25,26,37]

$$\nabla\left(\frac{1}{\rho_m}\nabla P_m\right)+\frac{\omega^2}{\rho_m c_m^2}P_m=0 \tag{18}$$

where a pressure formulation is considered to retain similarity with earlier studies [3,4]. In Eq. (18), P_m is the acoustic pressure and ρ_m and c_m are the equivalent density and speed of sound [29,30]. This version of the wave equation for non-uniform properties is consistent with the literature [3,4,25,26,37] and differs from the potential model of the central passage described in the previous section. For this mixed potential/pressure-based finite element approach, the coupling equations (between Ω_a and Ω_m) associated with the perforated duct present some differences compared to the usual finite element formulation. Further details will be given in section 2.4.

The finite element approach is applied to Eq. (18) with the resulting algebraic system being

$$\sum_{e=1}^{N_m^e}\left(\int_{\Omega_m^e}\frac{1}{\rho_m}\left(\nabla\mathbf{N}\right)^T\nabla\mathbf{N}\mathrm{d}\Omega-\omega^2\int_{\Omega_m^e}\frac{1}{\rho_m c_m^2}\mathbf{N}^T\mathbf{N}\mathrm{d}\Omega\right)\tilde{\mathbf{P}}_m^e=\sum_{e=1}^{N_m^e}\int_{\Gamma_m^e}\frac{1}{\rho_m}\mathbf{N}^T\frac{\partial P_m}{\partial n}\mathrm{d}\Gamma \tag{19}$$

where $\tilde{\mathbf{P}}_m^e$ contains the unknown nodal pressures and N_m^e represents the number of elements of subdomain Ω_m (absorbent material). In compact form Eq. (19) becomes

$$\left(\mathbf{K}_m-\omega^2\mathbf{M}_m\right)\tilde{\mathbf{P}}_m=\mathbf{F}_m \tag{20}$$

with the notation

$$\mathbf{K}_m = \sum_{e=1}^{N_m^e} \int_{\Omega_m^e} \frac{1}{\rho_m} \left(\nabla \mathbf{N}\right)^T \nabla \mathbf{N} \, \mathrm{d}\Omega, \qquad \mathbf{M}_m = \sum_{e=1}^{N_m^e} \int_{\Omega_m^e} \frac{1}{\rho_m c_m^2} \mathbf{N}^T \mathbf{N} \, \mathrm{d}\Omega \tag{21,22}$$

$$\mathbf{F}_m = \sum_{e=1}^{N_m^e} \int_{\Gamma_m^e \cap \Gamma_p} \frac{1}{\rho_m} \mathbf{N}^T \frac{\partial P_m}{\partial n} \mathrm{d}\Gamma \tag{23}$$

Details for the computation of the equivalent density and speed of sound ρ_m and c_m can be found in section 3. As in the case of the central passage, a temperature distribution will be assumed in the absorbent material.

2.3. Boundary conditions

The inlet and outlet sections Γ_i and Γ_o admit several boundary conditions in order to assess the acoustic attenuation performance of the silencer [33,38]. Velocity potential, acoustic velocity/pressure and impedance conditions can be applied. In practice, the former are directly introduced in the finite element equations, while Neumann and Robin conditions [36] are implemented taking into account the relations (2) and (4), repeated here for convenience,

$$\mathbf{U}_a = \nabla \Phi_a, \qquad U_a = \frac{\partial \Phi_a}{\partial x} \tag{24,25}$$

$$P_a = -\rho_a \, \mathrm{D}_t \Phi_a = -\rho_a \left(\frac{\partial \Phi_a}{\partial t} + U_{mf} \frac{\partial \Phi_a}{\partial x} \right) = -\rho_a \left(\mathrm{j}\omega \Phi_a + U_{mf} U_a \right) \tag{26}$$

The normal derivative of the potential along Γ_{bc} in the load vector $\mathbf{F}_a$ of Eq. (17) can be replaced by:

$$\frac{\partial \Phi_a}{\partial n} = \tilde{U}_a \qquad \text{Acoustic velocity condition} \tag{27}$$

$$\frac{\partial \Phi_a}{\partial n} = -\frac{\tilde{P}_a}{\rho_a U_{mf}} - \frac{\mathrm{j}\omega \Phi_a}{U_{mf}} \qquad \text{Acoustic pressure condition} \tag{28}$$

$$\frac{\partial \Phi_a}{\partial n} = -\frac{\rho_a \, \mathrm{j}\omega \Phi_a}{Z_a + \rho_a U_{mf}} \qquad \text{Anechoic termination (plane wave)} \tag{29}$$

where the tilde in $\tilde{P}_a$ and $\tilde{U}_a$ denotes a prescribed value and $Z_a = \rho_a \, c_a$.

2.4. Acoustic coupling at the perforated surface

The coupling between the central duct and the chamber is carried out by means of the acoustic impedance corresponding to the perforated surface. This impedance is defined as the ratio of the pressure difference to the normal acoustic velocity U_n [33]

$$\tilde{Z}_p = \frac{P_a - P_m}{U_n} \tag{30}$$

and depends, among others, on frequency, hole diameter, thickness, porosity, properties of the absorbent material and mean flow [39-41] (see details in section 3.2.). Eq. (30) includes both the acoustic pressure in the absorbent material P_m, which is the field variable explicitly contained in the wave equation (18), and the acoustic pressure in the air P_a, related to the velocity potential Φ_a of the convective wave equation (1) through the expression (26).

Several modelling possibilities can be considered regarding the acoustic phenomena close to perforated screen and the appropriate radial continuity conditions through the perforations [33,34,42-44]. Continuity of acoustic radial displacement/velocity are commonly found in the literature, and it has been experimentally demonstrated that a realistic condition is between displacement and velocity [43]. In view of the good correlation between prediction and experiment observed by Elnady *et al*. [44] using continuity of velocity and the numerical advantages of its implementation, this condition will be retained here for all the silencer transmission loss calculations. Therefore, the integral over Γ_p in the right side of the load vector $\mathbf{F}_a$ (see Eq. (17) for details) can be written in the form

$$\begin{aligned}\mathbf{F}_a &= \sum_{e=1}^{N_a^e} \int_{\Gamma_a^e \cap \Gamma_p} \rho_a \mathbf{N}^T \frac{\partial \Phi_a}{\partial n} \mathrm{d}\Gamma = \sum_{e=1}^{N_a^e} \int_{\Gamma_a^e \cap \Gamma_p} \rho_a \mathbf{N}^T \frac{P_a - P_m}{\tilde{Z}_p} \mathrm{d}\Gamma \\ &= \sum_{e=1}^{N_a^e} \int_{\Gamma_a^e \cap \Gamma_p} \rho_a \mathbf{N}^T \left(\frac{-\rho_a \mathrm{j}\omega \Phi_a - \rho_a U_{mf} \partial \Phi_a / \partial x}{\tilde{Z}_p} - \frac{P_m}{\tilde{Z}_p} \right) \mathrm{d}\Gamma\end{aligned} \tag{31}$$

In compact form, Eq. (31) becomes

$$\mathbf{F}_a = -\mathbf{K}_{aaZ_p} \tilde{\mathbf{\Phi}}_a - \mathbf{K}_{amZ_p} \tilde{\mathbf{P}}_m - \mathrm{j}\omega \mathbf{C}_{aaZ_p} \tilde{\mathbf{\Phi}}_a \tag{32}$$

where the following notation has been introduced

$$\mathbf{K}_{aaZ_p}=\sum_{e=1}^{N_a^e}\int_{\Gamma_a^e\cap\Gamma_p}\frac{\rho_a^2 U_{mf}\,\mathbf{N}^T}{\tilde{Z}_p}\frac{\partial\mathbf{N}}{\partial x}\mathrm{d}\Gamma\,,\qquad \mathbf{K}_{amZ_p}=\sum_{e=1}^{N_a^e}\int_{\Gamma_a^e\cap\Gamma_p}\frac{\rho_a\,\mathbf{N}^T\mathbf{N}}{\tilde{Z}_p}\mathrm{d}\Gamma \tag{33,34}$$

$$\mathbf{C}_{aaZ_p}=\sum_{e=1}^{N_a^e}\int_{\Gamma_a^e\cap\Gamma_p}\frac{\rho_a^2\,\mathbf{N}^T\mathbf{N}}{\tilde{Z}_p}\mathrm{d}\Gamma \tag{35}$$

Finally, from Eq. (23) the load vector $\mathbf{F}_m$ associated with the absorbent material yields

$$\begin{aligned}\mathbf{F}_m&=\sum_{e=1}^{N_m^e}\int_{\Gamma_m^e\cap\Gamma_p}\frac{1}{\rho_m}\mathbf{N}^T\frac{\partial P_m}{\partial n}\mathrm{d}\Gamma=\sum_{e=1}^{N_m^e}\int_{\Gamma_m^e\cap\Gamma_p}\frac{1}{\rho_m}\mathbf{N}^T\frac{\rho_m\,\mathrm{j}\omega\left(P_a-P_m\right)}{\tilde{Z}_p}\mathrm{d}\Gamma\\&=\sum_{e=1}^{N_m^e}\int_{\Gamma_m^e\cap\Gamma_p}\mathbf{N}^T\left(\frac{\rho_a\,\omega^2\,\Phi_a-\rho_a\,\mathrm{j}\omega U_{mf}\,\partial\Phi_a/\partial x}{\tilde{Z}_p}-\frac{j\omega P_m}{\tilde{Z}_p}\right)\mathrm{d}\Gamma\end{aligned} \tag{36}$$

The notation

$$\mathbf{C}_{mmZ_p}=\sum_{e=1}^{N_m^e}\int_{\Gamma_m^e\cap\Gamma_p}\frac{\mathbf{N}^T\mathbf{N}}{\tilde{Z}_p}\mathrm{d}\Gamma\,,\qquad \mathbf{C}_{maZ_p}=\sum_{e=1}^{N_m^e}\int_{\Gamma_m^e\cap\Gamma_p}\frac{\rho_a U_{mf}\,\mathbf{N}^T}{\tilde{Z}_p}\frac{\partial\mathbf{N}}{\partial x}\mathrm{d}\Gamma \tag{37,38}$$

$$\mathbf{M}_{maZ_p}=\sum_{e=1}^{N_m^e}\int_{\Gamma_m^e\cap\Gamma_p}\frac{\rho_a\,\mathbf{N}^T\mathbf{N}}{\tilde{Z}_p}\mathrm{d}\Gamma \tag{39}$$

leads to

$$\mathbf{F}_m=-\mathrm{j}\omega\mathbf{C}_{mmZ_p}\tilde{\mathbf{P}}_m-\mathrm{j}\omega\mathbf{C}_{maZ_p}\tilde{\mathbf{\Phi}}_a+\omega^2\mathbf{M}_{maZ_p}\tilde{\mathbf{\Phi}}_a \tag{40}$$

The calculation of acoustic impedance of the perforated surface in the presence of mean flow and temperature variations is presented in section 3.

2.5. Final system of equations

The combination of Eqs. (12), (20), (32) and (40) leads to the final system of equations

$$\left(\begin{bmatrix}\mathbf{K}_a+\mathbf{K}_{aaZ_p} & \mathbf{K}_{amZ_p}\\ \mathbf{0} & \mathbf{K}_m\end{bmatrix}+\mathrm{j}\omega\begin{bmatrix}\mathbf{C}_{a1}+\mathbf{C}_{a2}+\mathbf{C}_{aaZ_p} & \mathbf{0}\\ \mathbf{C}_{maZ_p} & \mathbf{C}_{mmZ_p}\end{bmatrix}-\omega^2\begin{bmatrix}\mathbf{M}_a & \mathbf{0}\\ \mathbf{M}_{maZ_p} & \mathbf{M}_m\end{bmatrix}\right)\begin{Bmatrix}\tilde{\mathbf{\Phi}}_a\\ \tilde{\mathbf{P}}_m\end{Bmatrix}=\begin{Bmatrix}\mathbf{F}_{a\_bc}\\ \mathbf{0}\end{Bmatrix} \tag{41}$$

The vector $\mathbf{F}_{a\_bc}$ is related to the inlet/outlet boundary conditions described in section 2.3. The application of acoustic velocity does not produce any additional mathematical issue, as can be inferred from Eqs. (17) and (27). Acoustic pressure and/or anechoic termination can be also implemented by considering Eqs. (28) and (29). In this case,

additional matrices have to be computed and incorporated in the damping matrix of Eq. (41).

3. TEMPERATURE-INDUCED PROPERTY VARIATIONS

3.1. Absorbent material. Spatial variations of the equivalent acoustic properties

Absorbent materials can be modelled as equivalent fluids [30] by using complex and frequency dependent values of speed of sound c_m and density ρ_m (or, equivalently, the characteristic impedance Z_m and wavenumber k_m). Empirical models such as the one proposed by Delany and Bazley [29] for rigid fibrous materials are commonly used to calculate c_m and ρ_m in terms of the steady airflow resistivity R. Once the resistivity is known, the equivalent acoustic properties can be expressed in terms of a number of coefficients a_i, i = 1, 2, ..., 8, derived from a curve fitting process following laboratory measurements, and the dimensionless frequency parameter $\xi = \rho_a f/R$, where ρ_a is the air density and f the frequency [30]. In the context of the current investigation, an extension is considered with $R = R(\mathbf{x})$; the frequency parameter is now a function of the coordinates ($\mathbf{x}$) so that the notation $\xi(\mathbf{x})$ is used. Therefore, the equivalent characteristic impedance Z_m and wavenumber k_m of the absorbent material are also a function of the spatial coordinates and can be calculated as [3,4,7]

$$Z_m(\mathbf{x}) = Z_a(\mathbf{x})\left(1 + a_5\,\xi(\mathbf{x})^{a_6} - \mathrm{j}a_7\,\xi(\mathbf{x})^{a_8}\right) \tag{42}$$

$$k_m(\mathbf{x}) = k_a(\mathbf{x})\left(1 + a_3\,\xi(\mathbf{x})^{a_4} - \mathrm{j}a_1\,\xi(\mathbf{x})^{a_2}\right) \tag{43}$$

$Z_a = \rho_a\, c_a$ being the characteristic impedance of the air and $k_a = \omega/c_a$ the associated wavenumber. Note that the coefficients and exponents a_i, i = 1, ..., 8, are considered constant, as in earlier works related to dissipative silencers [6,7]. Thus, the apparent difficulty associated with their possible temperature dependence has been dismissed. This is consistent with the high temperature results presented by Christie [28] and the recent experimental measurements carried out by Williams *et al.* [31], which have shown the validity of this hypothesis to provide an accurate prediction of the absorbent material properties.

Eqs. (42) and (43) are now used to evaluate the properties of the absorbent material for a given temperature distribution. A possible algorithm could be the following [6,7]. First, the properties of the air (ρ_a, c_a, Z_a and k_a) can be evaluated at each integration point assuming the ideal gas law. The local resistivity can be calculated from data at a reference temperature T_0 by means of the expression [20]

$$R\left(T\left(\mathbf{x}\right)\right)=R\left(T_0\right)\frac{\mu\left(T\left(\mathbf{x}\right)\right)}{\mu\left(T_0\right)} \tag{44}$$

where μ is the dynamic viscosity of the air (whose reference value can be approximated by $\mu(T_0)$ = 1.84·10^{-5} Pa·s for T_0 = 25 °C). For a continuously varying temperature field $T(\mathbf{x})$, the viscosity $\mu(T(\mathbf{x}))$ can be computed by means of the Sutherland's equation [45]

$$\mu\left(T\left(\mathbf{x}\right)\right)=1.458\cdot 10^{-6}\frac{\left(273.15+T\left(\mathbf{x}\right)\right)^{1.5}}{273.15+T\left(\mathbf{x}\right)+S} \tag{45}$$

where the Sutherland constant S is a characteristic of the gas (for air, a value of 110.4 K can be considered).

As the temperature increases, however, the combination of Eqs. (44) and (45) leads to an overestimation of the material resistivity in comparison with Christie's power law [28,31]

$$R\left(T\left(\mathbf{x}\right)\right)=R\left(T_0\right)\left(\frac{T\left(\mathbf{x}\right)+273.15}{T_0+273.15}\right)^{0.6} \tag{46}$$

For example, an approximate deviation of 10% has been found at 500 °C. Williams *et al.* [31] have recently provided further experimental validation to the use of Eq. (46). These authors have shown that the data measured at different temperatures collapse well onto Delany and Bazley curves if Eq. (46) is used for relating temperature and resistivity, and therefore the 0.6 power law will be used hereafter.

From Eqs. (42) and (43), the equivalent density and speed of sound are readily calculated as $c_m = \omega/k_m$ and $\rho_m = Z_m/c_m$. These values are introduced in the finite element integrals (21)-(23) to obtain the final system of equations (41). E glass and basalt wool

studied by Kirby and Cummings [46] are considered in this work, the relevant information being detailed in Table 1. The values $R(T_0)$ = 30716 rayl/m (E glass with filling density ρ_b = 120 kg/m^3) and $R(T_0)$ = 13813 rayl/m (basalt wool with ρ_b = 120 kg/m^3) are assumed. The information for a third absorbent material is also detailed in Table 1, corresponding to texturized fibre glass [32] with $R(T_0)$ = 4896 rayl/m for a filling density ρ_b = 100 kg/m^3.

Material	E glass	Basalt wool	Texturized fibre glass
a_1	0.220	0.218	0.1890
a_2	−0.585	−0.605	−0.595
a_3	0.201	0.128	0.160
a_4	−0.583	−0.675	−0.577
a_5	0.095	0.060	0.095
a_6	−0.669	−0.766	−0.754
a_7	0.169	0.138	0.085
a_8	−0.571	−0.628	−0.732

Table 1. Coefficients and exponents for the calculation of the equivalent acoustic properties.

3.2. Non-uniform acoustic impedance of the perforated surface

Some issues arise when a perforated duct, separating the central airway with mean flow and the absorbent material, is considered. First, how to evaluate the impact of the flow on the acoustic impedance of the perforations, and second, how to include the influence of the absorbent material. Both issues have been dealt with in the literature and a comprehensive review lies beyond the scope of this work. A number of references can be found regarding the acoustic behaviour of perforated ducts with grazing mean flow [20,33,39,41,47,48]. Good correlation with experimental results has been found in earlier studies [34] considering the model of Lee and Ih [47], which will be used in the current investigation.

According to Fig. 1, the central perforated passage is parallel to the x-axis, so that x is the only relevant coordinate when computing the acoustic impedance of the surface. Following the aforementioned work [47], the dimensionless impedance of a perforated screen with grazing mean flow is expressed here as

$$\zeta_p(x)=\frac{Z_p(x)}{\rho_a(x)c_a(x)}=\alpha(x)+\mathrm{j}\beta(x) \tag{47}$$

where the explicit dependence on x has been included for clarity. Note that the tilde has been intentionally omitted from the impedance $Z_p(x)$ in comparison with Eq. (30) to indicate that the effect of the absorbent material is not included on the acoustic behaviour of the perforations. The real and imaginary part of $\zeta_p(x)$ are given respectively by

$$\alpha(x)=\frac{\alpha_0\left(1+\alpha_1\left|f-f_{crit}(x)\right|\right)\left(1+\alpha_2 M(x)\right)\left(1+\alpha_3 d_h\right)\left(1+\alpha_4 t\right)}{\sigma} \tag{48}$$

$$\beta(x)=\frac{\beta_0\left(1+\beta_1 d_h\right)\left(1+\beta_2 t\right)\left(1+\beta_3 M(x)\right)\left(1+\beta_4 f\right)}{\sigma} \tag{49}$$

In Eqs. (48) and (49), $M(x)$ is the local mean flow Mach number, d_h the hole diameter, t_p the thickness, σ the porosity and f the frequency. In such a manner, the previous expressions are based on the assumption that the model of Lee and Ih [47] can be extended to situations where the mean flow Mach number varies with position. The critical value $f_{crit}(x)$ can be evaluated using the expression

$$f_{crit}(x)=\frac{\varphi_1\left(1+\varphi_2 M(x)\right)}{\left(1+\varphi_3 d_h\right)} \tag{50}$$

Lee and Ih [47] derived the coefficients from a curve fitting procedure to experimental data. The corresponding values are given in Table 2.

Real part (α)	Imaginary part (β)	f_{crit}
$\alpha_0 = 3.94\cdot10^{-4}$	$\beta_0 = -6.00\cdot10^{-3}$	$\varphi_1 = 412$
$\alpha_1 = 7.84\cdot10^{-3}$	$\beta_1 = 194$	$\varphi_2 = 104$
$\alpha_2 = 14.9$	$\beta_2 = 432$	$\varphi_3 = 274$
$\alpha_3 = 296$	$\beta_3 = -1.72$	––
$\alpha_4 = -127$	$\beta_4 = -6.62\cdot10^{-3}$	––

Table 2. Coefficients for the calculation of the acoustic impedance.

The above Eqs. (47)-(50), however, do not include the effect of the absorbent material on the acoustic impedance of the perforated duct. This influence has received attention in several works [39-41]. In reference [39], the effect of a fibrous material on the impedance of the perforated surface was measured and the authors suggested adding a correction to the impedance obtained in the absence of material. The correction is based on replacing the density of air with the equivalent density ρ_m. Lee et al. [40] also concluded that this procedure captures the effect of the absorbent material on the perforated duct. As shown in reference [34], good agreement between experimental and numerical silencer transmission loss is achieved considering an expression of the form

$$\tilde{Z}_p(x)=\rho_a(x)c_a(x)\left(\zeta_p(x)+\frac{\mathrm{j}0.425k_a(x)d_h\left(\rho_m(x)/\rho_a(x)-1\right)F(\sigma)}{\sigma}\right) \tag{51}$$

where the coordinate dependence has been included here to properly model the presence of heterogeneities in the material properties as well as in the mean flow Mach number. Note that the term $\zeta_p(x)$ is given by Eq. (47), and therefore the expression (51) considers simultaneously the influence of the mean flow and the absorbent material on the acoustic impedance of the perforated duct. To conclude, $F(\sigma)$ is related to the acoustic interaction between perforations and the following expression is considered [34,42,49]

$$F(\sigma)=1-1.055\sqrt{\sigma}+0.17\left(\sqrt{\sigma}\right)^3+0.035\left(\sqrt{\sigma}\right)^5 \tag{52}$$

3.3. Temperature field

The temperature distribution in the silencer is strongly related to a number of parameters, such as the geometrical configuration, thermal conductivities and convection heat transfer coefficients determining surface heat flux from the metallic housing to the surrounding air. In addition, convection coefficients depend on numerous fluid properties, flow conditions, vehicle speed and also the geometries of the surfaces involved [50]. Engine load and speed are relevant parameters as well, and significant temperature modifications can be found by running the engine at idle condition or accelerating to a certain speed. In Ref. [16], a method is developed for estimating the temperature profiles of the exhaust gases from the surface temperatures of the exhaust piping. Concerning the silencer, the corresponding axial temperature gradient $\Delta T_{ax} = T_i - T_o$ (T_i and T_o being the inlet and outlet temperatures, respectively) associated with different vehicle models is shown to vary over a wide interval. Engines running at idle and free accelerated conditions are considered. In this latter case, the particular ranges presented in Ref. [16] at a speed of

2000 rpm are 40 °C ~ 200 °C for ΔT_{ax}, 240 °C ~ 725 °C for T_i, and 200 °C ~ 650 °C for T_o. Reference [18] shows the axial temperature gradient along an exhaust system of a single-cylinder four-stroke engine. A reactive silencer is presented whose temperature variation is ΔT_{ax} = 200 °C approximately, with T_i = 510 °C and T_o = 315 °C. Transversal temperature variations ΔT_{rad} can be also significant in exhaust silencers, and thermal gradients higher than 100 °C can be found in the literature [17], resulting in complex profiles of the relevant acoustic properties.

The temperature and thermal gradients considered hereafter are based on values reported in the literature, although in some cases these have been exaggerated for a better illustration of their acoustic influence. Since the main purpose of the current investigation is to assess the impact of the thermal variations on the silencer performance, the temperature distributions used in the numerical computations are relatively simple and can be expressed analytically in terms of polynomial functions. Fig. 2 shows a sketch of the axisymmetric perforated dissipative silencer considered in the computations. As can be seen in the figure, the inlet and outlet sections are assumed to be at temperatures T_i and T_o, respectively. For the assessment of the thermal effects on the silencer performance, a linear temperature variation $T_{duct}(x)=b_0+b_1 x$ [6,7,9-13] can be assumed between the values T_i and T_o for the central passage carrying the axially-varying mean flow $M(x)$ [10,12,13]. At the outer chamber with absorbent material, the temperature varies according to the expression

$$T_{chamber}(x,r)=c_0+c_1 x+c_2 r+c_3 xr+c_4 r^2+c_5 xr^2 \tag{53}$$

combining a linear variation along the axial direction and a quadratic law in the radial coordinate, defined from the values T_{ri}, i = 1, 2, ..., 6. Note that this quadratic function is used to interpolate the approximate logarithmic temperature distribution through a cylindrical domain [50]. To evaluate the acoustic impedance $\tilde{Z}_p(x)$ of the perforated surface at a given position, the average of $T_{duct}(x)$ and $T_{chamber}(x,r = R_1)$ could be used. The temperature difference between both sides of the perforated surface [17] is expressed as $\Delta T_p(x) = T_{duct}(x) - T_{chamber}(x,r = R_1)$. For simplicity, in all the computations hereafter the value ΔT_p = 0 is assumed, that is, $T_i = T_{r1}$ and $T_o = T_{r4}$.

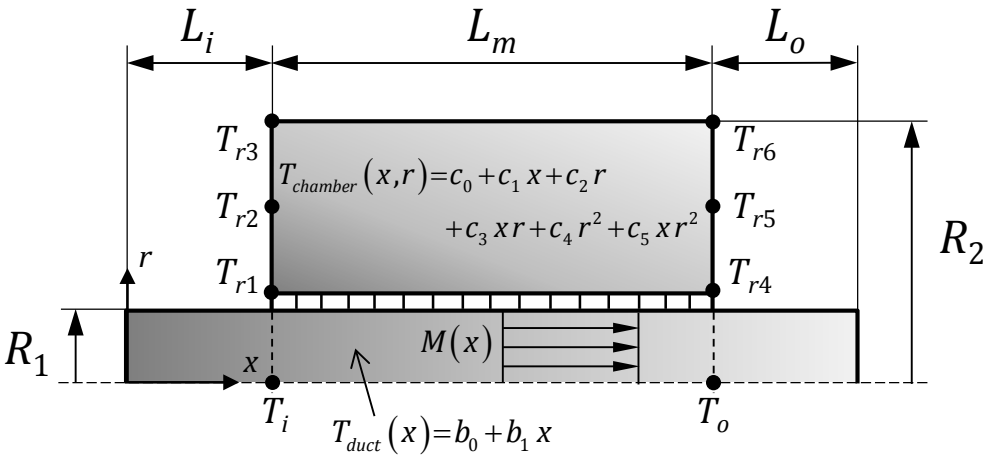

Figure 2 – Axisymmetric geometry under analysis and temperature distributions.

4. RESULTS

The problem under study consists of an axisymmetric configuration whose relevant dimensions are L_m = 0.3 m, R_1 = 0.0268 m and R_2 = 0.091875 m (see Fig. 2). In addition, the values L_i = L_o = 0.1 m are used in the finite element discretizations to guarantee plane wave propagation conditions in the inlet/outlet sections [33]. Transmission loss computations have been carried out using 8-noded axisymmetric quadrilateral elements with quadratic interpolation, the FE meshes having an approximate element size of 0.0075 m to provide an accurate solution in the frequency range under analysis. Results for the three absorbent materials detailed in Table 1 (E glass, basalt wool and texturized fibre glass) will be presented in the next sections. The mean flow is defined by the Mach number M_i at the silencer inlet section, obtaining the local value $M(x)$ from continuity of mass flow. The parameters that characterize the perforated duct are: porosity σ = 0.2, thickness t_p = 0.001 m and hole diameter d_h = 0.0035 m. These values are considered in all the calculations hereafter.

4.1 Influence of temperature and axial gradients

The influence of temperature and the corresponding axial thermal gradients are assessed first. For comparison purposes, radial temperature variations are not included in this analysis, that is, ΔT_{rad} = 0 °C. The relevant information associated with the first temperature distributions is provided in Table 3, including the values T_i, T_o and T_{ri}, i = 1, 2, ..., 6 shown in Fig. 2, and the average temperature in the absorbent material. In the three

cases under analysis, the same temperature is considered at the outlet section (200 °C), while the inlet temperature increases from 300 °C (Case aI) to 400 °C (Case aII) and 500 °C (Case aIII). Thus, the values of the axial temperature gradients for the computations are ΔT_{ax} = 100 °C, 200 °C and 300 °C, respectively. The inlet mean flow Mach number is given by M_i = 0.1.

	T_i (°C)	T_o (°C)	T_{r1} (°C)	T_{r2} (°C)	T_{r3} (°C)	T_{r4} (°C)	T_{r5} (°C)	T_{r6} (°C)	T_{avg} (°C)
Case aI	300	200	300	300	300	200	200	200	250
Case aII	400	200	400	400	400	200	200	200	300
Case aIII	500	200	500	500	500	200	200	200	350

Table 3. Definition of the temperature field, Cases aI-aIII.

Fig. 3 depicts the transmission loss curves of Cases aI-aIII for a perforated dissipative silencer containing basalt wool (see material details in Table 1). Predictions presented here also include two calculations for uniform temperature fields. The former is T_{unif} = 25 °C (ΔT_{ax} = ΔT_{rad} = 0 °C) and corresponds to the usual "cold condition" found in the literature [1-5, 32-35], while the latter is given by T_{unif} = 200 °C (the value considered for the outlet temperature in Cases aI-aIII) to illustrate the impact of an increasing mean temperature and axial gradient in high temperature situations. For validation purposes, the mixed approach (potential/pressure) presented here is compared with a pressure-based formulation valid in the absence of flow [7] for the particular axial temperature gradient associated with Case aI.

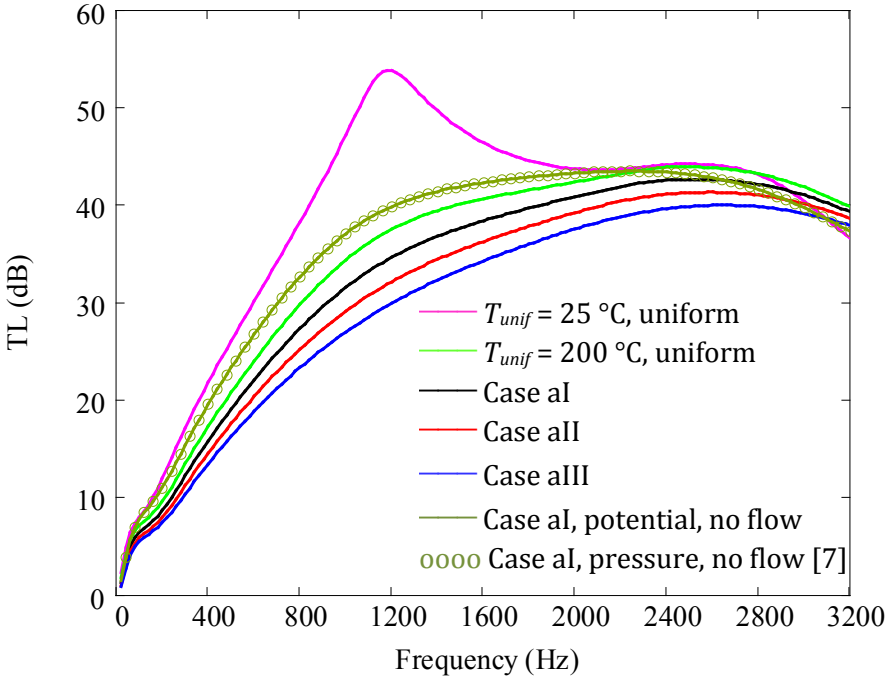

Figure 3 – TL of a perforated dissipative silencer containing basalt wool with different temperature distributions.

The transmission loss predictions delivered by the mixed formulation presented here and the predictions given by the pressure formulation [7] are almost undistinguishable and an excellent agreement is obtained. As can be seen in the figure, a significant change in the silencer performance is observed as the temperature varies. A comparison between the transmission loss curves for uniform temperature fields (T_{unif} = 25 °C and T_{unif} = 200 °C) confirms the conclusions of previous studies [6,7], that is, predictions for dissipative configurations at cold conditions can differ significantly from the results at high temperature and the use of a normalized frequency f/c does not provide the transmission loss overlapping found in reactive geometries. In principle, the influence of the thermal gradient seems also relevant in the curves depicted in the figure, since increasing values of ΔT_{ax} lead to a deterioration of the attenuation in the frequency range of analysis. However, with Cases aI-aIII the mean temperature changes as well, the values being T_{avg} = 250 °C, T_{avg} = 300 °C and T_{avg} = 350 °C, respectively. Thus, the effect of the temperature gradient is not isolated and it is difficult to discern exactly what is affecting the silencer performance.

Therefore, further computations are required, the analysis being extended with the temperature distributions detailed in Table 4. Note that for these new calculations the temperature at the outlet section is not the same and now the axial gradients of Cases aIV and aV lead to an average temperature that equals the mean value of Case aI, that is, T_{avg} = 250 °C

	T_i (°C)	T_o (°C)	T_{r1} (°C)	T_{r2} (°C)	T_{r3} (°C)	T_{r4} (°C)	T_{r5} (°C)	T_{r6} (°C)	T_{avg} (°C)
Case aIV	350	150	350	350	350	150	150	150	250
Case aV	400	100	400	400	400	100	100	100	250

Table 4. Definition of the temperature field, Cases aIV and aV.

Fig. 4 shows the results of Cases aI, aIV and aV, again for a silencer containing basalt wool. A computation with uniform temperature field (T_{unif} = 250 °C) is also included for comparison. The inlet mean flow Mach number is given by M_i = 0.1.

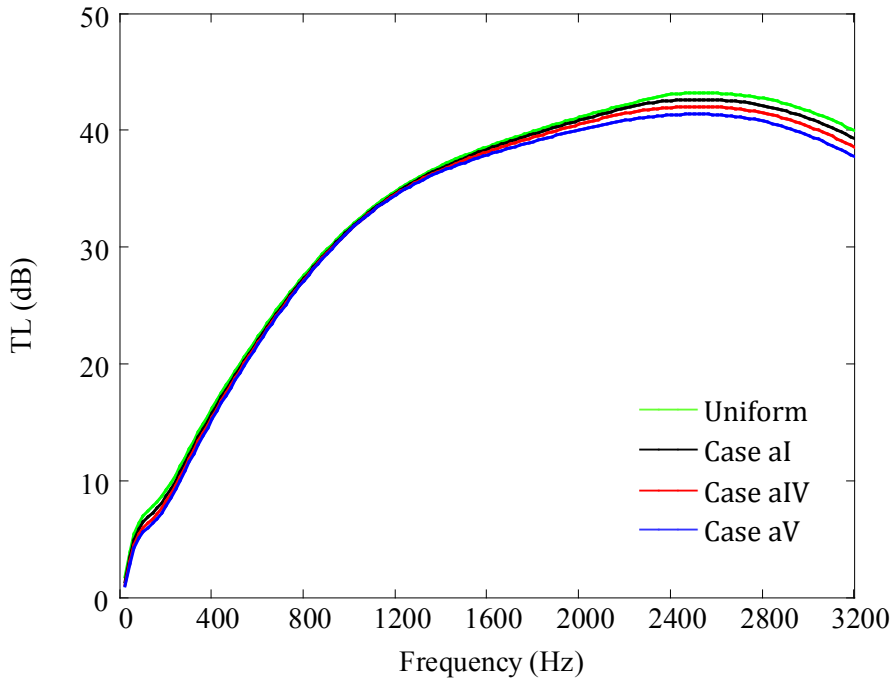

Figure 4 – TL of a perforated dissipative silencer containing basalt wool with different temperature distributions and equal average value T_{avg} = 250 °C.

As can be seen in the figure, higher values of ΔT_{ax} lead to a slight deterioration of the attenuation in the high frequency range, while no significant impact of the axial gradient is found at low and mid frequencies, even when the gradients used in the computations are considerable. The differences are now lower compared to those found in Fig. 3, since only the influence of the gradient is taken into account, the mean temperature effect being omitted. Note that, for the cases under consideration, ignoring the presence of the temperature gradient is likely to provide a slight overestimation of the silencer performance. The maximum transmission loss difference is found between the uniform temperature distribution and Case aV, the value being approximately 5% (TL = 39.9 dB and TL = 37.7 dB at 3200 Hz, respectively). Thus, when designing the silencer it seems that it is only necessary to include the presence of axial temperature gradients and the associated thermal effects if accurate predictions are required in the high frequency range, while an average temperature provides a reasonable estimation at lower frequencies. A similar analysis will be presented in section 4.2 related to radial gradients. The assessment of a simplified approach with transmission loss computations considering the average temperature in the presence of general axial and radial gradients will be provided in Section 4.3.

Material resistivity is likely to be a very influential property when modelling thermal effects. Comparing the temperature distributions detailed in Table 3, it is clear that there are significant differences. In particular, as indicated previously, the average values are T_{avg} = 250 °C, T_{avg} = 300 °C and T_{avg} = 350 °C, for Cases aI, aII and aIII, respectively. From Eq. (46), an increase in the average resistivity of the absorbent material is obtained for higher mean temperatures. Table 5 provides the corresponding average values over the dissipative region for the three materials considered in this work.

	R_{avg} (rayl/m) Basalt wool	R_{avg} (rayl/m) Texturized fibre	R_{avg} (rayl/m) E glass
Case aI	19348	6858	43025
Case aII	20420	7238	45408
Case aIII	21447	7602	47691

Table 5. Average resistivity for the absorbent materials, Cases aI-aIII.

Further transmission loss results are shown in Fig. 5 considering Cases aI-aIII for texturized fibre glass and E glass. As shown in Table 5, the former is less resistive than basalt wool, while the latter exhibits a higher resistivity. The value M_i = 0.1 is used in the computations.

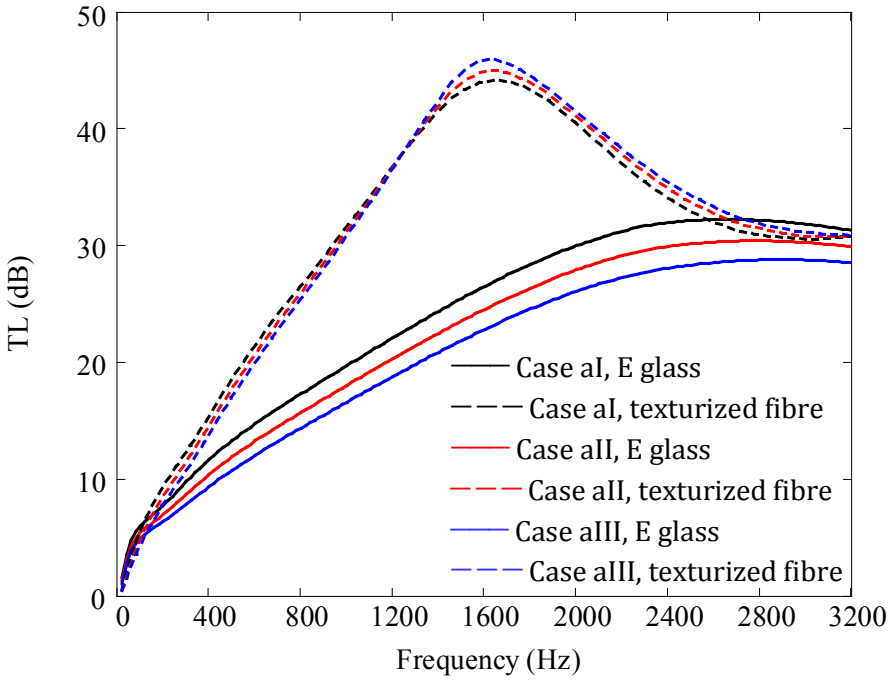

Figure 5 – TL of a perforated dissipative silencer with different temperature distributions.

The attenuation delivered by the configurations containing texturized fibre glass improves the results associated with E glass in almost all the frequency range. For this latter material with higher resistivity, a worse acoustic performance is found as the average temperature and the axial gradient increase, as previously observed for basalt wool in Figs. 3 and 4. Considering the texturized fibre glass, it is worth noting that the combined impact of increasing mean temperature and the associated gradient is less pronounced than in the case of basalt wool and E glass. For this less resistive material, a slight drop in the silencer performance is observed initially when changing from Case aI to Case aIII, up to a transition frequency of approximately 1250 Hz. Beyond this transition frequency, however, the assessment of the acoustic behaviour shows a slight improvement, the silencer seeming more effective at attenuating sound for Case aIII. Further computations (not presented here) show that the aforementioned transition frequency

also appears for higher material resistivities (E glass and basalt wool), but the associated frequencies are beyond the frequency limits considered in the current work.

Isolating the influence of the axial gradient for E glass and texturized fibre (Cases aIV and aV) delivers the transmission loss curves depicted in Fig. 6. As in Fig. 4, Case aI as well as a computation with uniform temperature field (T_{unif} = 250 °C) are also included for comparison. As in the previous figures, the inlet mean flow Mach number is given by M_i = 0.1.

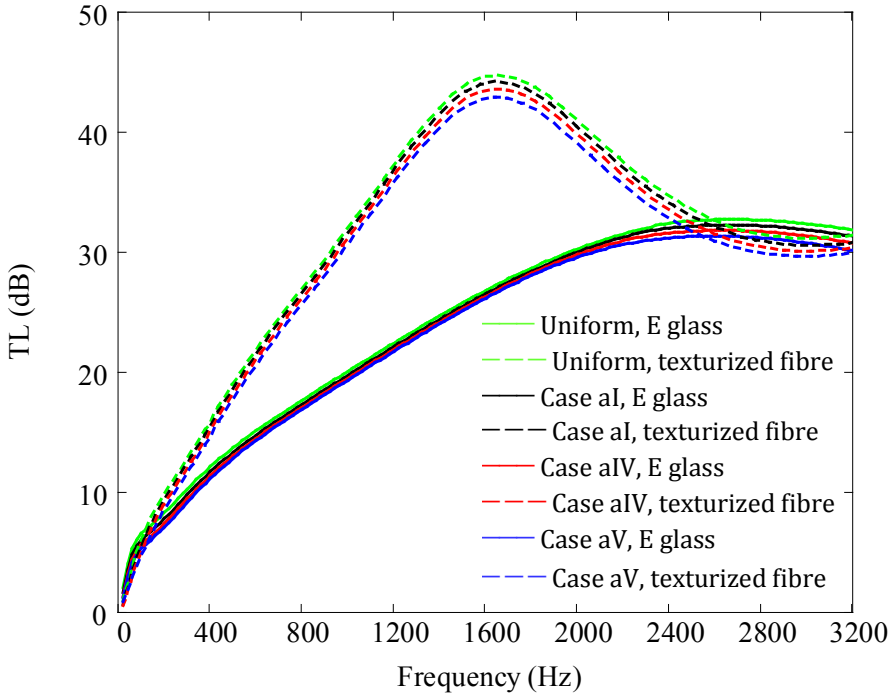

Figure 6 – TL of a perforated dissipative silencer with different temperature distributions and equal average value T_{avg} = 250 °C.

For both materials, higher values of ΔT_{ax} lead to a slight detrimental effect on the silencer transmission loss, mainly in the high frequency range. Attenuation overestimations up to 5% are obtained in the computations if the axial temperature gradient is neglected. This value is similar to the previous results found in Fig. 4 for basalt wool. Note that, from Figs. 3 and 5, it was concluded that the average temperature has a great impact on the attenuation when using high resistivity materials, while its effect is

smaller for low material airflow resistivity. For the axial gradient considered separately (Figs. 4 and 6), a lower influence is found in general, more concentrated in the high frequency range, and the resistivity does not seem to play such an important role.

4.2 Impact of radial thermal variations

Table 6 provides the temperature values T_i, T_o and T_{ri}, i = 1, 2, ..., 6, considered to analyse the influence of temperature and corresponding radial thermal variations (with ΔT_{ax} = 0 °C). The temperature at the outer surface (with $r = R_2$) is the same in these three first cases under study, its value being 200 °C. The increases $\Delta T_{rad} = T_{r1} - T_{r3}$ are 50 °C, 100 °C and 150 °C for Cases bI, bII and bIII, respectively. Information is also provided regarding the average temperature in the absorbent material. The central values T_{r2} and T_{r4} are obtained by approximating a logarithmic temperature distribution along the radial coordinate [50]. As in the previous section, the inlet mean flow Mach number is M_i = 0.1.

	T_i (°C)	T_o (°C)	T_{r1} (°C)	T_{r2} (°C)	T_{r3} (°C)	T_{r4} (°C)	T_{r5} (°C)	T_{r6} (°C)	T_{avg} (°C)
Case bI	250	250	250	218	200	250	218	200	216
Case bII	300	300	300	235	200	300	235	200	231
Case bIII	350	350	350	253	200	350	253	200	247

Table 6. Definition of the temperature field, Cases bI-bIII.

The transmission loss computations for E glass are shown in Fig. 7, including a configuration with uniform temperature T_{unif} = 200 °C (the value considered for the outer surface with $r = R_2$ in Cases bI-bIII). As can be observed in the figure, the results are consistent with the previous computations of section 4.1. with high temperature and axial gradient and the influence on the attenuation of the temperature and the associated radial gradient is relevant. Temperature rise leads to a detrimental reduction of the acoustic performance. The silencer attenuation is seen to drop as the temperature and thermal gradient are higher. A possible reason may be associated with a saturation effect due to the high resistivity of E glass, which increases as the average temperature rises, and partially prevents the sound energy from penetrating the material in the frequency range under analysis.

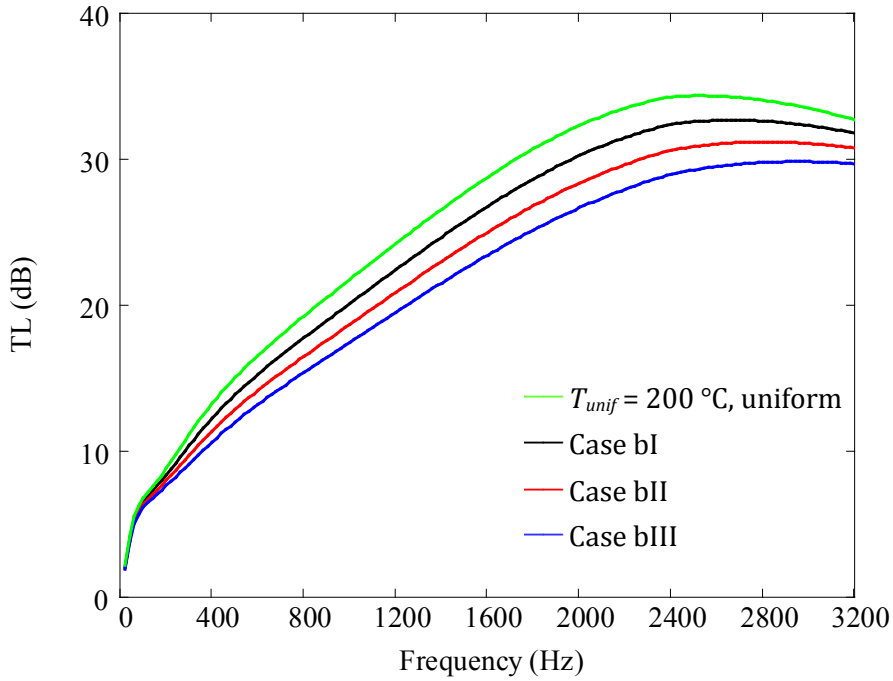

Figure 7 – TL of a perforated dissipative silencer containing E glass with different temperature distributions.

To analyse the impact of the radial temperature gradient separately, Cases bIV and bV are now considered, with the temperature distributions detailed in Table 7. An average temperature of 231 °C, similar to the mean value of Case bII, is taken into account.

	T_i (°C)	T_o (°C)	T_{r1} (°C)	T_{r2} (°C)	T_{r3} (°C)	T_{r4} (°C)	T_{r5} (°C)	T_{r6} (°C)	T_{avg} (°C)
Case bIV	410	410	410	242	150	410	242	150	231
Case bV	520	520	520	249	100	520	249	100	231

Table 7. Definition of the temperature field, Cases bIV and bV.

Fig. 8 shows the results of Cases bII, bIV and bV for a silencer containing E glass, as well as the attenuation curve provided by a computation with uniform temperature field (T_{unif} = 231 °C). According to the figure, relevant differences between the transmission loss predictions can be obtained. As opposite to the case of the axial gradient, there are now significant discrepancies resulting from the radial temperature variations, extended over the entire frequency range. It is evident in Fig. 2 that neglecting the radial temperature

gradient ΔT_{rad} can lead to a systematic overprediction of the silencer performance, the effect being stronger as the radial thermal variation increases.

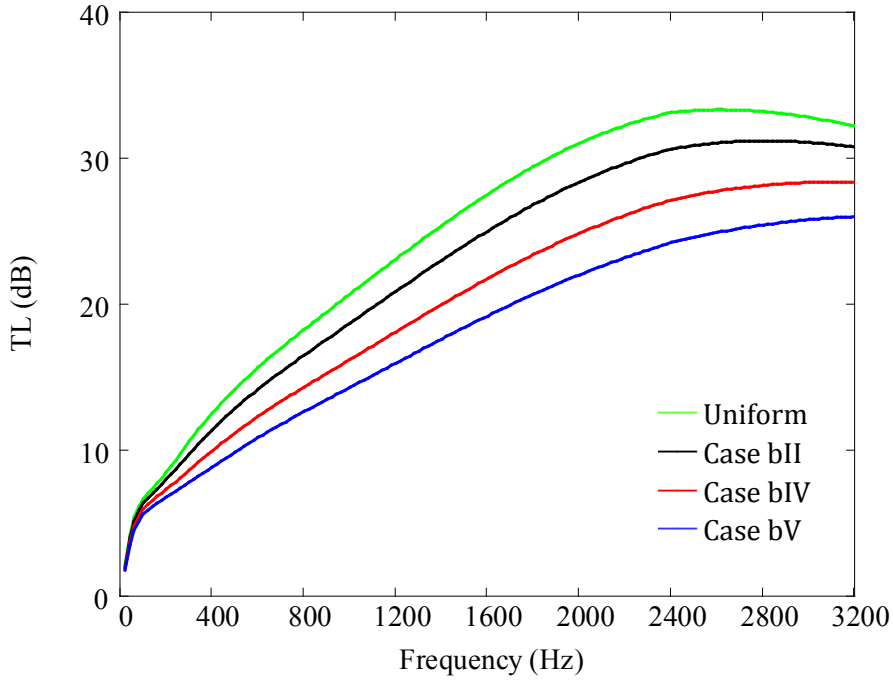

Figure 8 – TL of a perforated dissipative silencer containing E glass with different temperature distributions and equal average value T_{avg} = 231 °C.

The particular values corresponding to the attenuation overestimation in Fig. 8 are detailed next. The configuration with uniform temperature field is taken as reference for comparison. Considering first Case bII, the maximum transmission loss variation is 9% at 1980 Hz. For Case bIV, an approximate discrepancy of 20% appears at 2060 Hz, while differences up to 28% are obtained with Case V at 2160 Hz. Thus, using an average temperature for the computations does not necessarily provide accurate acoustic predictions in the cases under study. Note that, although the particular values of radial temperature gradient used for bIV and bV cases are exaggerated on purpose, the heat transfer through the outer shell can be considerable, therefore justifying the need to include transverse temperature variations in the silencer noise attenuation calculations.

In Fig. 9, a comparison between predictions for Cases bII, bIV and bV is made considering texturized fibre glass. A configuration with uniform temperature having equal

average value (231 °C) is also included. The predictions appear be quite similar in the frequency region depicted, with only some relevant differences close to 1500 Hz. At low frequencies, higher gradients lead to a systematic reduction of the attenuation performance, while an irregular influence is found at mid to high frequency values. Thus, previous conclusions obtained from Fig. 8 for the combination of radial gradient and E glass no longer hold for low material airflow resistivity, since only a slight influence of the radial gradient is found in general.

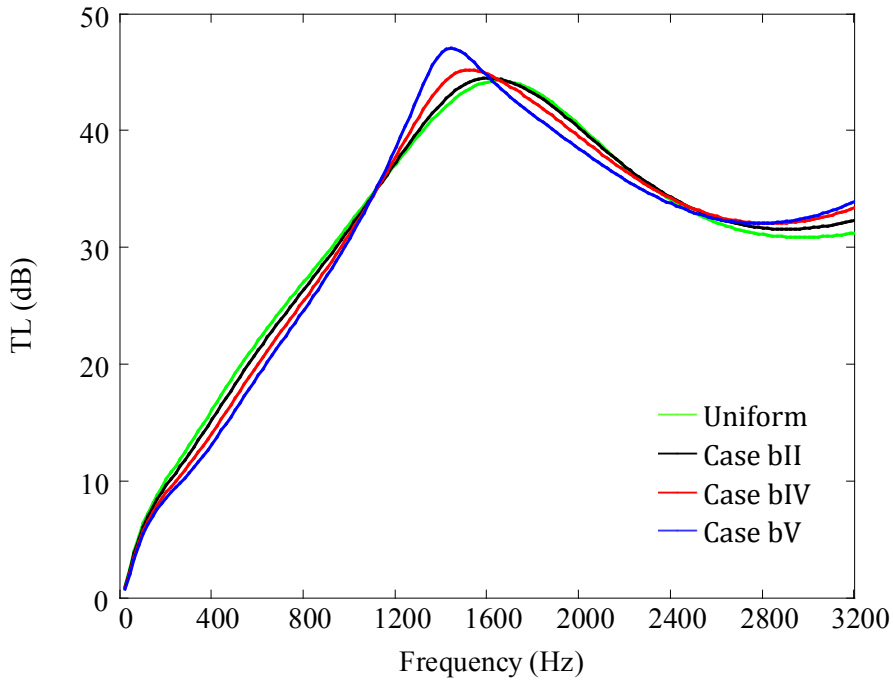

Figure 9 – TL of a perforated dissipative silencer containing texturized fibre glass with different temperature distributions and equal average value T_{avg} = 231 °C.

4.3 General temperature fields and TL computations with average value

More general temperature distributions are analysed in this section, where axial and radial temperature gradients are considered simultaneously through the values T_i, T_o and T_{ri}, i = 1, 2, ..., 6 provided in Table 8. In all the configurations under study, the average temperature over the absorbent material is the same, given by T_{avg} = 185 °C. An examination of the previous results in sections 4.1. and 4.2 shows axial thermal gradients providing a slight acoustic impact in general and radial temperature variations having a more relevant influence for medium to high material airflow resistivities. Therefore, it is

expected that the simultaneous presence of both gradients will modify the silencer attenuation performance for basalt wool and E glass considered here, while texturized fibre will exhibit a smaller effect. It is worth assessing if predictions for uniform temperature computations based on the average value compare well with results corresponding to non-uniform temperature fields including axial and radial thermal variations. If so, this would be a suitable simplified approach to compute the transmission loss of silencers with temperature gradients.

	T_i (°C)	T_o (°C)	T_{r1} (°C)	T_{r2} (°C)	T_{r3} (°C)	T_{r4} (°C)	T_{r5} (°C)	T_{r6} (°C)	T_{avg} (°C)
Case cI	300	200	300	210	160	200	168	150	185
Case cII	400	200	400	254	175	200	129	90	185

Table 8. Definition of the temperature field, Cases cI and cII.

Figure 10 depicts the transmission loss computations for Cases cI and cII considering texturized fibre and E glass. The sound attenuation associated with a uniform temperature field defined by T_{avg} = 185 °C is also calculated for comparison purposes. The inlet mean flow Mach number in the computations is M_i = 0.1. As expected, different trends are found depending on the material. For the low resistivity configuration (texturized fibre glass), the maximum discrepancy between the different predictions is approximately 2 dB, thus confirming the limited impact of the thermal gradient and justifying the use of a simplified approach with an average temperature value. For the high resistivity case (E glass) it is worth noting that, even when the average temperature in the absorbent material is approximately the same for all the computations, the attenuation overestimation assuming uniform temperature field can be considerable. This effect is stronger as the temperature gradients are higher; for example, the maximum TL discrepancy between the uniform temperature field and Case cI is about 3 dB, while a difference higher than 5 dB is found between the uniform temperature predictions and Case cII at 1920 Hz. These latter results seem to indicate that, for general temperature fields including radial gradients in relatively resistive materials, an accurate and reliable prediction of the attenuation performance cannot be guaranteed if an average temperature value is considered.

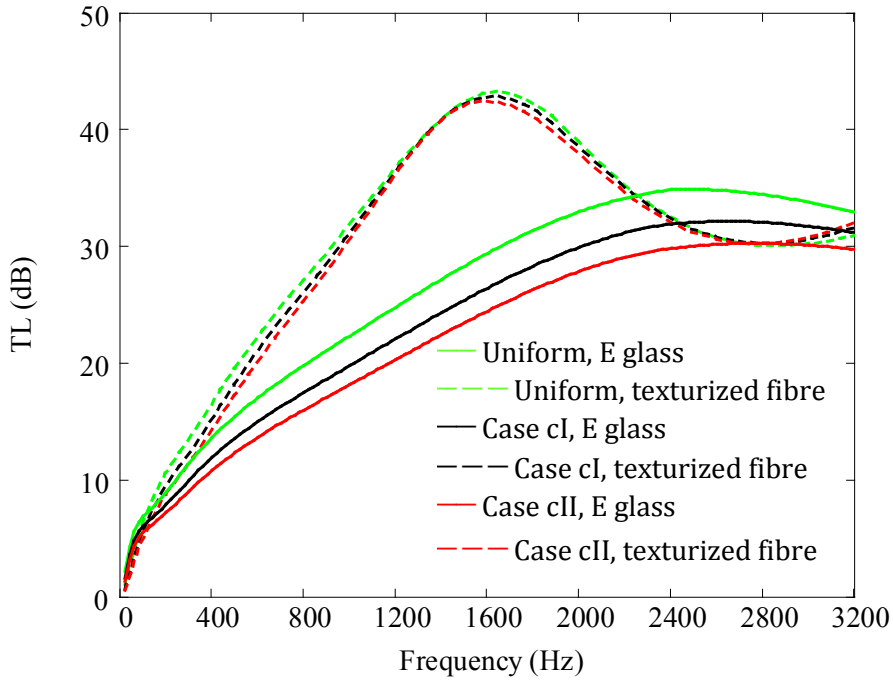

Figure 10 – TL of a perforated dissipative silencer with different temperature distributions and equal average value T_{avg} = 185 °C.

4.4 Mean flow considerations

Computations are carried out in this section including several inlet mean flow Mach numbers given by M_i = 0, 0.1 and 0.2 and the temperature distributions described in Table 9, where axial and radial temperature gradients are considered simultaneously. The particular axial values analysed here are ΔT_{ax} = 100 °C and 200 °C for Cases dI and dII, respectively, while the radial temperature variation is ΔT_{rad} = 100 °C in all the calculations. Note that the temperature distribution at the outlet section is the same in the two configurations under analysis (defined by T_{r4}, T_{r5} and T_{r6}). The results for basalt wool and the temperature distributions corresponding to Cases dI and dII are presented in Fig. 11.

	T_i (°C)	T_o (°C)	T_{r1} (°C)	T_{r2} (°C)	T_{r3} (°C)	T_{r4} (°C)	T_{r5} (°C)	T_{r6} (°C)	T_{avg} (°C)
Case dI	400	300	400	335	300	300	235	200	281
Case dII	500	300	500	435	400	300	235	200	331

Table 9. Definition of the temperature field, Cases dI and dII.

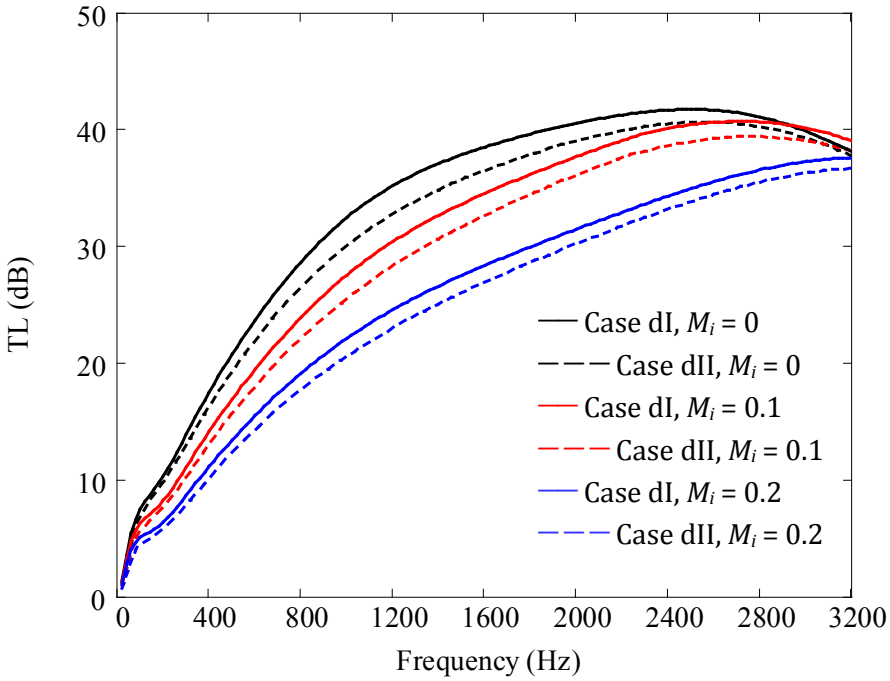

Figure 11 – TL of a perforated dissipative silencer containing basalt wool with different temperature distributions and mean flow.

In general, increasing the inlet Mach number while keeping the same temperature field yields a detrimental influence of the mean flow in almost all the frequency range under consideration, except in the highest part of the interval depicted in the figure. This is consistent with earlier results [34] obtained in the presence of mean flow at room temperature, that is, an increase in flow velocity leads to a drop in the silencer performance. For a given inlet mean flow, higher average temperature and thermal gradients lead to lower attenuation in the frequency interval considered. However, the transition frequency for the case with M_i = 0 has shifted to lower frequencies and it is slightly higher than 3200 Hz (the intersection between the solid black line and dash black line can be inferred from the figure). This transition shifts towards higher frequencies beyond the figure limits as the mean flow velocity rises. Note that, for a given thermal field, as the temperature decreases along the central passage, opposite density and speed of sound variations take place, resulting in a small reduction between the inlet and outlet Mach numbers.

CONCLUSIONS

A finite element model has been derived for the acoustic analysis of perforated dissipative silencers with high temperature and thermal gradients in the presence of mean flow. The spatial variations of the temperature field have been shown to generate heterogeneities in the mean flow as well as in the properties of the sound propagation media (air and absorbent material). For the central passage, an acoustic velocity potential-based wave equation has been considered, valid for non-uniform mean flow and inhomogeneous fluid (air) with properties that vary with position. Concerning the outer chamber, the absorbent material has been modelled by its complex equivalent acoustic properties. The temperature-induced variations of these properties have been evaluated through a heterogeneous temperature-dependent resistivity in combination with absorbent material models obtained at room temperature. A pressure-based wave equation valid for variable properties and stationary medium has been then used with the equivalent density and speed of sound varying as functions of the spatial coordinates. The acoustic connection between the central passage and the outer chamber has been carried out by means of the acoustic impedance of the perforated duct. The dependence of this impedance on the heterogeneous properties of the absorbent material and the non-uniform mean flow has led to a spatial variation of the acoustic coupling and also to additional convective terms in the governing equations.

Several computational predictions have been obtained considering different temperature fields and mean flow Mach numbers in combination with a number of absorbent materials. A detailed analysis of the silencer performance has shown that, for an accurate prediction, it is necessary to include the temperature effects when modelling the acoustic behaviour. For high material flow resistivity, increasing mean temperature have been shown to deliver a general reduction in the sound attenuation. Similar conclusions have been found for axial and radial thermal gradients, although axial temperature variations have exhibited a reduced impact. Therefore, a suitable representation of the thermal effects is required to avoid an overestimation of the silencer performance. For less resistive materials, an increase in temperature and/or thermal gradient has led to a slight drop in the silencer performance in the low to mid frequency range but the opposite trend has been found at higher frequencies, the transition point shifting to higher frequencies as the temperature gradient and/or mean flow rise. In general, for some silencer configurations it may be relatively accurate to approximate the temperature field by using a uniform profile considering an average value. It has been shown, however, that this is not always possible, the model implemented here being primarily intended for use with bulk

materials having medium to high airflow resistivities. In this latter case, attenuation overestimation is likely to be predicted if the temperature distribution is not taken into account, justifying the current numerical implementation. Finally, the influence of the mean flow on the transmission loss is consistent with earlier results obtained at room temperature, with higher Mach numbers leading to a drop in the silencer performance.

ACKNOWLEDGEMENTS

Authors gratefully acknowledge the financial support of Ministerio de Economía y Competitividad (projects DPI2010-15412 and TRA2013-45596-C2-1-R), Generalitat Valenciana (project Prometeo/2012/023) and Universitat Politècnica de València (PAID-05-12, project SP20120452).

REFERENCES

[1] A. Selamet, M. B. Xu, I. J. Lee, N. T. Huff, Dissipative expansion chambers with two concentric layers of fibrous materials, *Int. J. Veh. Noise Vib.* 1 (2005) 341-357.

[2] A. Selamet, M. B. Xu, I. J. Lee, N. T. Huff, Effects of voids on the acoustics of perforated dissipative silencers, *Int. J. Veh. Noise Vib.* 2 (2006) 357-372.

[3] A. G. Antebas, F. D. Denia, A. M. Pedrosa, F. J. Fuenmayor, A finite element approach for the acoustic modeling of perforated dissipative mufflers with non-homogeneous properties, *Math. Comput. Model.* 57 (2013) 1970-1978.

[4] E. M. Sánchez-Orgaz, F. D. Denia, J. Martínez-Casas, L. Baeza, 3D acoustic modelling of dissipative mufflers with nonhomogeneous properties and mean flow, *Adv. Mech. Eng.* (2014) in press.

[5] K. S. Peat, K. L. Rathi, A finite element analysis of the convected acoustic wave motion in dissipative silencers, *J. Sound Vib.* 184 (1995) 529-545.

[6] F. D. Denia, A. G. Antebas, J. Martínez-Casas, F. J. Fuenmayor, Transmission loss calculations for dissipative mufflers with temperature gradients, *Proc. ICA 2010, 20th Int. Congr. Acoust.*, Sydney, August 2010, pp. 2117-2122.

[7] F. D. Denia, F. J. Fuenmayor, A. J. Torregrosa, A. Selamet, Numerical modelling of thermal effects on the acoustic attenuation of dissipative mufflers, *Proc. Inter-noise 2012, 41st Int. Congr. Expo. Noise Control Eng.*, New York, August 2012, pp. 1548-1559.

[8] S. B. Dong, C. Y. Liu, A finite-element analysis of sound propagation in a nonuniform moving medium, *J. Acoust. Soc. Am.* 66 (1979) 548-555.

[9] M. G. Prasad, M. J. Crocker, Evaluation of four-pole parameters for a straight pipe with a mean flow and a linear temperature gradient, *J. Acoust. Soc. Am.* 69 (1981) 916-921.

[10] M. L. Munjal, M. G. Prasad, On plane-wave propagation in a uniform pipe in the presence of a mean flow and a temperature gradient, *J. Acoust. Soc. Am.* 80 (1986) 1501-1506.

[11] R. I. Sujith, Transfer matrix of a uniform duct with an axial mean temperature gradient, *J. Acoust. Soc. Am.* 100 (1996) 2540-2542.

[12] E. Dokumaci, Transmission of sound in uniform pipes carrying hot gas flows, *J. Sound Vib.* 195 (1996) 257-266.

[13] B. Karthik, B. M. Kumar, R. I. Sujith, Exact solutions to one-dimensional acoustic fields with temperature gradient and mean flow, *J. Acoust. Soc. Am.* 108 (2000) 38-43.

[14] F. Payri, A. J. Torregrosa, R. Payri, Evaluation through pressure and mass velocity distributions of the linear acoustical description of I.C. engine exhaust systems, *Appl. Acoust.* 60 (2000) 489-504.

[15] H. S. Han, S. S. Chae, Y. C. Kim, Analytical design of muffler based on transmission loss calculation, *FISITA World Automot. Congr.*, Seoul, June 2000, SAE Paper 2000-05-0311, pp. 1-6.

[16] M. Ehsan, M. Z. Shah, M. Hasan, S. M. R. Hasan, Study of temperature profile in automotive exhaust systems for retrofitting catalytic converters, *Proc. Int. Conf. Mech. Eng.*, Dakha, December 2005, ICME05-TH-34, pp. 1-6.

[17] X. Hou, X. Guo, Z. Liu, F. Yan, F. Pen, Flow Field Analysis and Improvement of Automobile Exhaust System Cold End, *Int. Conf. Comput. Intel. Softw. Eng.*, Wuhan, December 2010, pp. 1-5.

[18] L. J. Eriksson, *Silencers*, in: D. E. Baxa (Ed.), *Noise Control in Internal Combustion Engines*, Wiley, New York, 1982, pp. 238-292.

[19] R. H. Paulino, F. A. Rochinha, A higher-order velocity post-processing for the Hemlholtz equation, *Finite Elem. Anal. Des.* 41 (2005) 459-492.

[20] F. P. Mechel, *Formulas of Acoustics*, Springer, Berlin, 2004.

[21] Y. H. Kim, J. W. Choi, B.D. Lim, Acoustic characteristics of an expansion chamber with constant mass flow and steady temperature gradient (theory and numerical simulation), *J. Vib. Acoust.* 112 (1990) 460-467.

[22] Y. H. Kim, J. W. Choi, General solution of acoustic wave equation for circular reversing chamber with temperature gradient, *J. Vib. Acoust.* 113 (1991) 543-550.

[23] C. N. Wang, Y. N. Chen, J. Y. Tsai, The application of boundary element evaluation on a silencer in the presence of a linear temperature gradient, *Appl. Acoust.* 62 (2001) 707-716.

[24] D. Siano, Three-dimensional/one-dimensional numerical correlation study of a three-pass perforated tube, *Simul. Model. Pract. Theor.* 19 (2011) 1143-1153.

[25] A. D. Pierce, Wave equation for sound in fluids with unsteady inhomogeneous flow, *J. Acoust. Soc. Am.* 87 (1990) 2292-2299.

[26] Z. Wan, T. Wang, Q. Huang, J. Wang, Acoustic finite element model updating using acoustic frequency response function, *Finite Elem. Anal. Des.* 87 (2014) 1-9.

[27] LMSVirtual.Lab Rev. 11, LMS International, Leuven, Belgium, 2012.

[28] D. R. A. Christie, Measurement of the acoustic properties of a sound absorbing material at high temperatures, *J. Sound Vib.* 46 (1976) 347-355.

[29] M. E. Delany, E. N. Bazley, Acoustical properties of fibrous absorbent materials, *Appl. Acoust.* 3 (1970) 105-116.

[30] J. F. Allard, N. Atalla, *Propagation of Sound in Porous Media: Modelling Sound Absorbing Materials*, Wiley, Chichester, 2009.

[31] P. Williams, R. Kirby, C. Malecki and J. Hill, Measurement of the bulk acoustic properties of fibrous materials at high temperatures, *Appl. Acoust.* 77 (2014) 29-36.

[32] A. Selamet, I. J Lee, N.T Huff, Acoustic attenuation of hybrid silencers, *J. Sound Vib.* 262 (2003) 509-527.

[33] M. L. Munjal, *Acoustics of Ducts and Mufflers*, Wiley, New York, 2014.

[34] R. Kirby, F. D. Denia, Analytic mode matching for a circular dissipative silencer containing mean flow and a perforated pipe, *J. Acoust. Soc. Am.* 122 (2007) 3471-3482.

[35] R. Kirby, A comparison between analytic and numerical methods for modelling automotive dissipative silencers with mean flow, *J. Sound Vib.* 325 (2009) 565-582.

[36] O. C. Zienkiewicz, R. L. Taylor, J. Z. Zhu, *The Finite Element Method: Its Basis and Fundamentals*, Elsevier Butterworth-Heinemann, Burlington, 2005.

[37] J. E. Murphy, S. A. Chin-Bing, A finite-element model for ocean acoustic propagation and scattering, *J. Acoust. Soc. Am.* 86 (1989) 1478-1483.

[38] K. S. Peat, Evaluation of four-pole parameters for ducts with flow by the finite element method, *J. Sound Vib.* 84 (1982) 389-395.

[39] R. Kirby, A. Cummings, The impedance of perforated plates subjected to grazing gas flow and backed by porous media, *J. Sound Vib.* 217 (1998) 619-636.

[40] I. J. Lee, A. Selamet, N. T. Huff, Acoustic impedance of perforations in contact with fibrous material, *J. Acoust. Soc. Am.* 119 (2006) 2785-2797.

[41] I. J. Lee, A. Selamet, Measurement of acoustic impedance of perforations in contact with absorbing material in the presence of mean flow, *Noise Control Eng. J.* 60 (2012) 258-266.

[42] J. L. Bento, Acoustic characteristics of perforate liners in expansion chambers (Ph. D. Thesis), University of Southampton, 1983.

[43] Y. Aurégan, M. Leroux, Failures in the discrete models for flowduct with perforations: an experimental investigation, *J. Sound Vib.* 265 (2003) 109-121.

[44] T. Elnady, M. Åbom, S. Allam, Modeling perforates in mufflers using two-ports, *J. Vib. Acoust.* 132 (2010) 1-11.

[45] H. Schlichting, *Boundary-Layer Theory*, McGraw-Hill, New York, 1979.

[46] R. Kirby, A. Cummings, Prediction of the bulk acoustic properties of fibrous materials at low frequencies, *Appl. Acoust.* 56 (1999) 101-125.

[47] S. H. Lee, J. G. Ih, Empirical model of the acoustic impedance of a circular orifice in grazing mean flow, *J. Acoust. Soc. Am.* 114 (2003) 98-113.

[48] N. S. Dickey, A. Selamet, M. S. Ciray, An experimental study of the impedance of perforated plates with grazing flow, *J. Acoust. Soc. Am.* 110 (2001) 2360-2370.

[49] F. D. Denia, A. Selamet, F. J. Fuenmayor, R. Kirby, Acoustic attenuation performance of perforated dissipative mufflers with empty inlet/outlet extensions, *J. Sound Vib.* 302 (2007) 1000–1017.

[50] F. P. Incropera, D. P. Dewitt, T. L. Bergman, A. S. Lavine, *Principles of Heat and Mass Transfer* , Wiley, Singapore, 2013.